

Geophysical joint inversion using statistical petrophysical constraints and prior information

Jérémie Giraud*

Centre for Exploration
Targeting (University of
Western Australia)
35, Stirling Highway
WA Crawley 6009, Australia
Jeremie.giraud@research.uwa.
edu.au

Mark Jessell

Centre for Exploration
Targeting (University of
Western Australia)
35, Stirling Highway
WA Crawley 6009, Australia
mark.jessell@uwa.edu.au

Mark Lindsay

Centre for Exploration
Targeting (University of
Western Australia)
35, Stirling Highway
WA Crawley 6009, Australia
mark.lindsay@uwa.edu.au

Roland Martin

Géoscience Environnement
Toulouse
Observatoire Midi-Pyrenees
14 Avenue Edouard Belin
31400 Toulouse, France
roland.martin@get.obs-mip.fr

Evren Pakyuz-Charrier

Centre for Exploration
Targeting (University of
Western Australia)
35, Stirling Highway
WA Crawley 6009, Australia
evren.pakyuz-
charrier@research.uwa.edu.au

Vitaliy Ogarko

Centre for Exploration
Targeting (University of
Western Australia)
35, Stirling Highway
WA Crawley 6009, Australia
vitaliy.ogarko@uwa.edu.au

SUMMARY

We introduce and test a workflow that integrates petrophysical constraints and geological data in joint geophysical inversion in order to decrease the uncertainty of the results. This workflow uses statistical petrophysical properties to constrain the values retrieved by the geophysical inversion and geological prior information to decrease the effect of non-uniqueness. We integrate the different sources of information in a Bayesian framework, which takes into account the state of information. This permits us to quantify the posterior state of knowledge, the reduction of the uncertainty and to calculate the influence of prior information using quality indicators based on fixed-point statistics. This workflow was first tested using simple synthetic datasets to validate the method and assess the robustness of the workflow. As a result, the use of petrophysical constraints permits us to retrieve sharper boundaries, while prior structural information from geology permits to retrieve the geometry more accurately. Overall, the integration of the different constraints provides a model, with reduced uncertainties and better resolved parameters.

Key words: geoscience integration, joint inversion, uncertainty, petrophysical constraints, prior information.

INTRODUCTION

Context and motivations

In recent years, the integration of different geophysical techniques has been of growing importance in natural resources exploration and production due to the necessity to 1) exploit the complementarity between methods in increasingly challenging scenarios and 2) reduce the risk of costly development of low-productivity deposits and reservoirs. Previous studies have developed joint inversion techniques focusing on structural constraints to enforce structural similarity between the different models (Gallardo and Meju, 2003; Colombo and De Stefano, 2007). Others studies focused on the use of constitutive petrophysical laws to link the different domains (Gao et al., 2012).

More recently, Sun and Li (2012, 2013) have introduced clustering algorithms as a means to enforce similarities between values in the inverted model and petrophysical data; Zhang and Revil (2015) show the integration of petrophysical clustering and geological data in joint inversion. However, even if the objective of the approaches quoted above is to obtain better constrained models, as mentioned by Reid et al. (2013), little work has been done to quantify the uncertainty or the resolving power of these techniques. In this abstract we present a workflow integrating single domain and constrained joint inversion procedures to accurately assess uncertainty changes.

We constrain the joint inversions using petrophysical constraints in the same spirit as the clustering approaches introduced by Sun and Li (2012), but also further the method by integrating prior geological information. We formulate the problem in a Bayesian framework in order to quantify the posterior uncertainties and confidence levels in the results. The approach we follow allows the inversion to produce results that are statistically consistent with petrophysical measurements. Before using the algorithm on complex, realistic cases we tested and validated the workflow using a synthetic model. As a result, the use of petrophysical constraints in joint geophysical inversion permits us to retrieve petrophysical properties accurately while honouring geophysical data. Moreover, the integration of petrophysical constraints and the use of geological prior information increases the level of confidence in the results. Therefore, we conclude that integration of petrophysical, geological and geophysical information reduces uncertainty.

Workflow summary

The workflow integrates various sources of information to constrain geophysical inversion in order to reduce uncertainty and to address the under-determination of the problem. Geological prior information is used to create the starting models. Geological modelling carries geological uncertainty in the form of covariance matrices that control how the model is updated by geophysical inversion. Petrophysical data is used in a statistical framework to constrain the values taken by the model during inversion.

In the joint inversion workflow constrained single domain inversions are performed first. The results of single domain inversions are then used as a source of prior information for joint inversion. This allows us to retrieve improved starting models for joint inversion and to obtain an updated model covariance matrix for each domain. The workflow as applied to gravity and magnetic data is summarised in Figure 1.

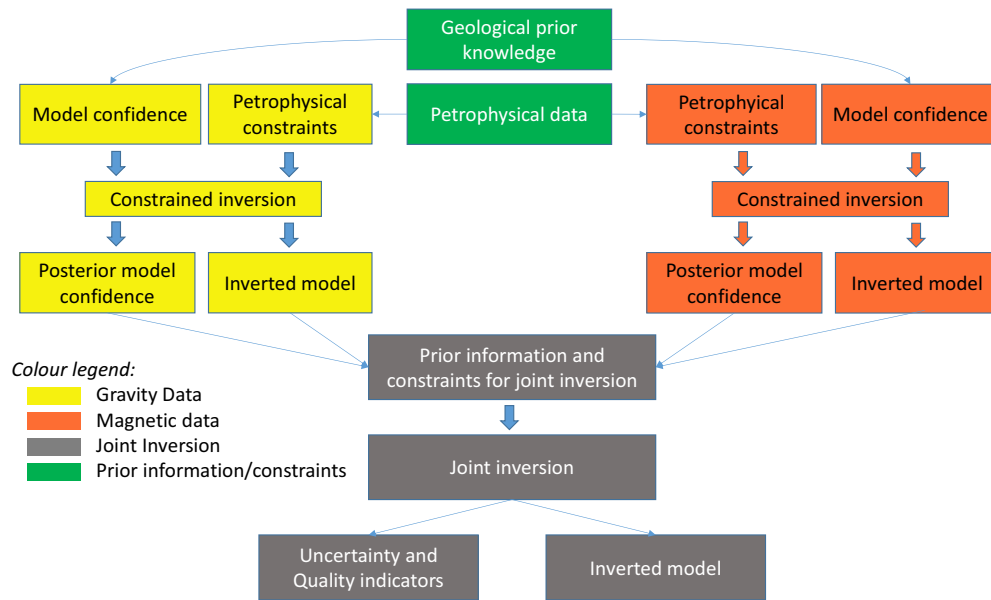


Figure 1: Integrated joint inversion workflow. This illustrates the interaction between single domain inversion (yellow and red) as an additional source of prior information.

THEORY AND METHODS

Inversion framework

We chose to formulate the inverse problem using the framework introduced by Tarantola and Valette (1982) in a least-squares sense for its ability to account for multiple sources of prior information and constraints. We minimize the following misfit function (equation (1)):

$$\theta(\mathbf{m}) = (\mathbf{g}(\mathbf{m}) - \mathbf{d})^T \mathbf{C}_d^{-1} (\mathbf{g}(\mathbf{m}) - \mathbf{d}) + (\mathbf{m} - \mathbf{m}_0)^T \mathbf{C}_m^{-1} (\mathbf{m} - \mathbf{m}_0) + (\mathbf{P}_{max} - \mathbf{P}(\mathbf{m}))^T \mathbf{C}_p^{-1} (\mathbf{P}_{max} - \mathbf{P}(\mathbf{m})) \quad (1)$$

where θ is the function to be minimised. \mathbf{m} represents the model while \mathbf{d} represents the measurements. \mathbf{g} is the operator that calculates the data model \mathbf{m} produces. \mathbf{m}_0 is the starting model. \mathbf{C}_m and \mathbf{C}_d are the model covariance and data covariance matrices, respectively. \mathbf{C}_p is what we call the probability covariance matrix. \mathbf{P} is the function calculating the probability of occurrence of a given model \mathbf{m} . \mathbf{P}_{max} contains the probability of occurrence of the optimum model for perfect knowledge. Superscript T denotes the transpose operator.

The first two terms in equation (1) relate to data and model misfit, respectively. The third term relates to the probability of occurrence of the model based on external sources of information.

We minimize $\theta(\mathbf{m})$ using a quasi-Newton damped least-squares algorithm in the same fashion as Garofalo et al. (2015), who follow the work of Tarantola (1987). The model is updated using a fixed-point method as follows (equation (2)):

$$\mathbf{m}_{k+1} = \mathbf{m}_k + [\mathbf{G}_k^T \mathbf{C}_d^{-1} \mathbf{G}_k + \mathbf{C}_m^{-1} + \mathbf{J}_k^T \mathbf{C}_p^{-1} \mathbf{J}_k + \mathbf{C}_p^{-1} + \lambda \mathbf{I}]^{-1} [\mathbf{G}_k^T \mathbf{C}_d^{-1} (\mathbf{d}_0 - \mathbf{g}(\mathbf{m}_k)) - \mathbf{C}_m^{-1} (\mathbf{m}_k - \mathbf{m}_0) + \mathbf{J}_k^T \mathbf{C}_p^{-1} (\mathbf{P}_{max} - \mathbf{P}(\mathbf{m}_k))] \quad (2)$$

where \mathbf{G}_k and \mathbf{J}_k are, respectively, the matrices of the partial derivatives of \mathbf{g} and \mathbf{P} with respect to the model \mathbf{m} . Subscript k denotes the k -th iteration. λ is the damping parameter and \mathbf{I} is the identity matrix.

Formulation of the petrophysical constraints

The petrophysical constraints are applied through the minimization of the third term of equation (1) simultaneously to the minimization of the data and model misfit terms. To enforce the petrophysical constraints we follow ideas introduced by Sun and Li (2012) on petrophysical clustering. In the workflow presented in this abstract we assume that the petrophysical properties are normally distributed for each rock type. Therefore, \mathbf{P} can be formulated as a mixture model. The distribution describing the rock types is inferred from borehole and surface measurements. $\mathbf{P}(\mathbf{m})$ is expressed as:

$$\mathbf{P}(\mathbf{m}) = \sum_{k=1}^{n_f} \omega_k \mathbf{N}(\mathbf{m} | \boldsymbol{\mu}_k, \boldsymbol{\sigma}_k) \quad (3)$$

where n_f is the number of rock types (or facies) in the observations that are used to estimate the properties of the normal distributions \mathbf{N} : the mean value $\boldsymbol{\mu}_k$ and covariance matrix $\boldsymbol{\sigma}_k$. ω_k is the weight assigned to the k -th facies in the mixture defining \mathbf{P} . $\boldsymbol{\mu}_k$ and $\boldsymbol{\sigma}_k$ are fitted to each individual rock type petrophysical data. ω_k are obtained from a prior probabilistic geological model.

Use of prior information and single domain inversion

Geological information is used to calculate several terms in equation (1). The variance of the model and the degree of correlation between the different units in the model is used to populate the initial model covariance matrix \mathbf{C}_m . In addition geological information is also used as a source of prior information to build \mathbf{C}_p and the starting model \mathbf{m}_0 . The confidence level in the starting model and variability of the associated model is also embedded in the model covariance matrix. Geostatistical modelling provides such information.

The inverted models from single domain inversion are used for the joint inversion. The associated posterior model covariance matrices are used as input to the joint inversion. Intermediate models (e.g. before full convergence is reached) can also be used as starting model. Prior information is also embedded in \mathbf{P} as it is defined using petrophysical data.

Application to joint inversion

The methodology introduced above can be applied to joint inversion provided that the different properties inverted for can be linked. In our case the degree of linkage between these properties is determined by the mixture model and by the non-diagonal elements of $\boldsymbol{\sigma}_k$ (equation (3)). The dimensions of \mathbf{P} and \mathbf{J} vary accordingly to the number of datasets inverted jointly. That is, the dimension of the mixture model is exactly the same as the number of geophysical data types inverted.

The models for each domain of the joint inversion are updated separately using equation (2), with the contribution of the link between the different domains (terms relating to \mathbf{P} in equation (2)) modifying the resulting search direction. This is illustrated in Figure 2. The resulting models would fit both data and petrophysical constraints.

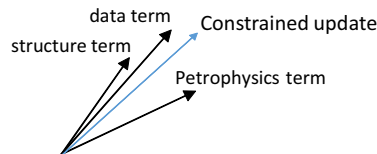


Figure 2: Contribution of the different terms to search direction in model space. The search direction is the weighted average of the search directions minimizing equation (1), taking into account equation (2) and (3).

Calculating posterior uncertainty and resolution indicator

We assess the quality of the inversion results by analysing the posterior covariance matrix and the resolution matrix. We calculate these indicators by adapting the methodology used by Soueid Ahmed et al. (2014) who invert jointly hydraulic heads and self-potential data. The posterior covariance matrix \mathbf{C}_{post} is calculated as follows (equation (4)):

$$\mathbf{C}_{post} = \mathbf{C}_m - \begin{bmatrix} \mathbf{H} \cdot \mathbf{C} \\ \mathbf{U}^T \end{bmatrix} \begin{bmatrix} \mathbf{H} \cdot \mathbf{C} \cdot \mathbf{H}^T + \mathbf{V} & \mathbf{H}\mathbf{U} \\ (\mathbf{H}\mathbf{U})^T & \mathbf{0} \end{bmatrix}^{-1} \begin{bmatrix} \mathbf{H}\mathbf{U} \\ \mathbf{U}^T \end{bmatrix} \quad \text{where} \quad \begin{cases} \mathbf{H} = [\mathbf{G}, \mathbf{J}]^T \\ \mathbf{C} = [\mathbf{C}_m, \mathbf{C}_p]^T \\ \mathbf{U} = \mathbf{1} \\ \mathbf{V} = \begin{bmatrix} \mathbf{C}_d & \mathbf{0} \\ \mathbf{0} & \boldsymbol{\sigma} \end{bmatrix} \end{cases} \quad (4)$$

Where $\boldsymbol{\sigma}$ is that matrix containing the covariance parameters used to define \mathbf{P} .

The resolution matrix \mathbf{R} is calculated as follows (equation (5)):

$$\mathbf{R} = \left[\mathbf{H}^T \mathbf{V}^{-1} \mathbf{H}^T + \mathbf{C}_p^{-1} - \mathbf{C}_p^{-1} \mathbf{U} [\mathbf{U}^T \mathbf{C}_p^{-1} \mathbf{U}]^{-1} \mathbf{U} \mathbf{C}_p^{-1} \right]^{-1} \mathbf{H}^T \mathbf{V} \mathbf{H}^{-1} \quad (5)$$

EXAMPLES AND RESULTS

Synthetic model

We generate gravity and magnetic data using a simple model made of two anomalous bodies encased in homogeneous host rock. To test the algorithm on diverse types of anomalies we create a small, shallow body and a larger, deeper one. The small body simulates low-density mafic intrusion and the larger one represents a felsic intrusion. The anomalies are characterized by a positive contrast of 0.2 g/cc and a magnetic susceptibility of 0.1 SI.

We assume that the cross-plot data of density and magnetic susceptibility obtained from surface and borehole measurements can be modelled using a mixture model using equation (3). The mixture model (MM) we generate is Gaussian. It is characterized by a standard deviation of 0.02 g/cc along the density contrast axis and 0.016 SI along the magnetic susceptibility axis. The mean values of the Gaussians in the MM are zero g/cc and zero SI and 0.2 g/cc and 0.1 SI, respectively. We also assume a covariance of 0.1 in σ_k . We assign the weights introduced in equation (3) accounting for the facies repartition expected from geology.

The investigated model and the Gaussian MM are shown on Figure 3.

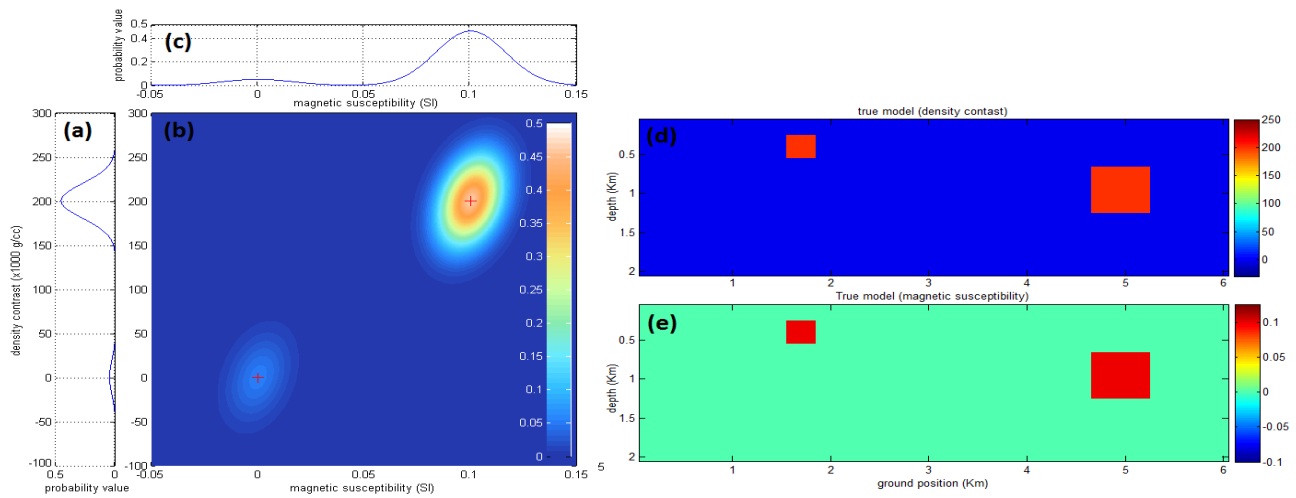


Figure 3: Plot of the Gaussian MM (a) Gaussian MM used for single domain gravity data inversion in $Kg.m^{-3}$ (b) Gaussian MM used for joint inversion (c) Gaussian mixture for single domain magnetic data inversion, SI. (d) and (e) True petrophysical model used to generate geophysical data. The cell-size is 100m*100m and the size of the model is 60*20 cells.

We simulated gravity data acquired with relative gravimeters at regular intervals. We simulated airborne magnetic data at the same horizontal position as the gravity data points but at different altitudes.

Joint inversion

As mentioned in the previous section we use the results obtained from single domain inversion as a starting model and as a source of prior information for the joint inversion. Figure 4 shows the starting model and the result of joint inversion.

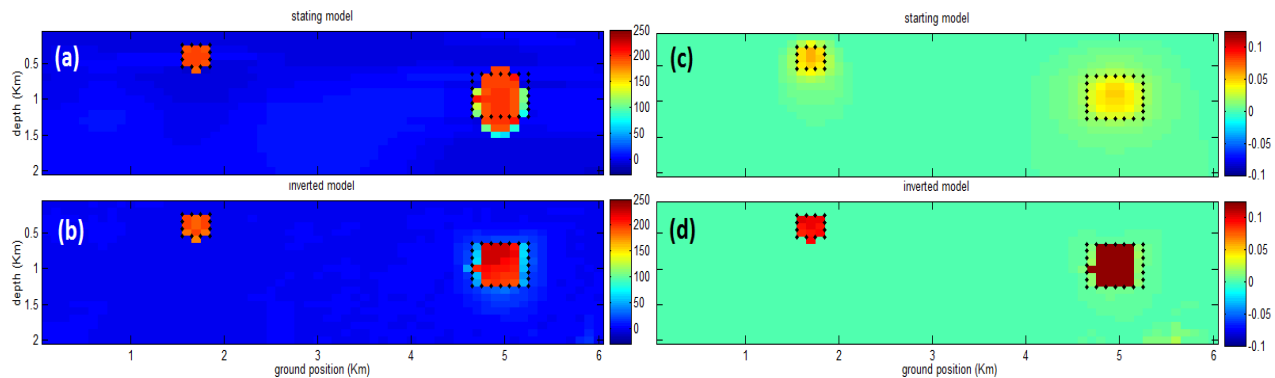


Figure 4: Starting and inverted density contrast models ((a) and (b), respectively), and starting and inverted magnetic susceptibility ((c) and (d), respectively). The black dots show the edges of the true model.

In Figure 4 the sharpness of the starting model is due to the petrophysical clustering constraints that have been applied on single domain inversion. As can be seen in Figure 4, joint inversion refines the model and sharpens it further. The geometry of the inverted model is improved and the values of the model are closer to the true model.

Results indicate that the use of the petrophysical constraints improves the focusing of the anomalies even on single domain inversion. The retrieved values are closer to the true model than the “usual” potential field inversions where the anomalies are usually quite smooth.

Uncertainty and resolution analysis

From the calculation of the posterior model covariance matrix and the prior model covariance matrix we extract the difference between the latter two variances for each cell of the model. This provides a visual indicator of the decrease of the variance of the model due to the joint inversion. Another indicator can be obtained by extracting “resolution sections” from the diagonal elements of the resolution matrix.

The resolution sections and the variance reduction are shown on Figure 5.

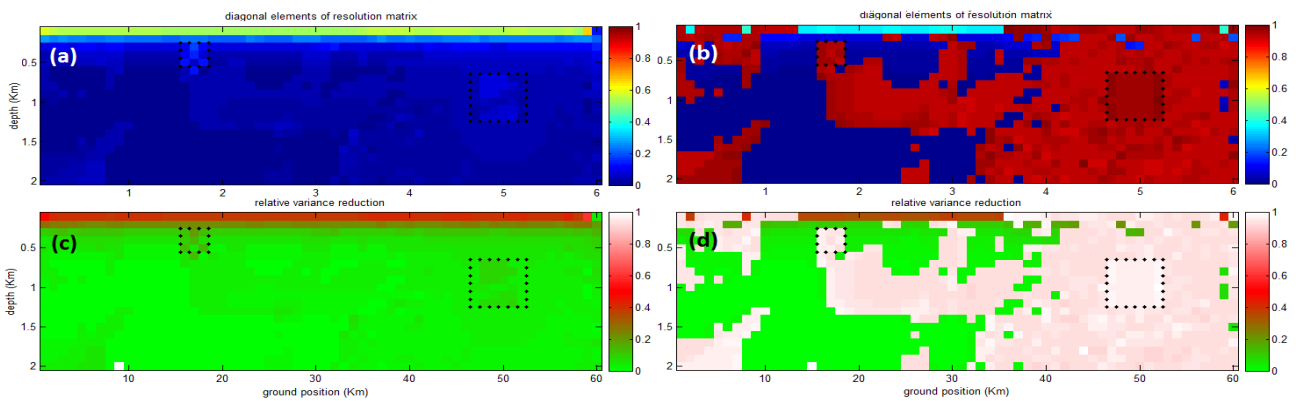


Figure 5: Resolution section of magnetic susceptibility (a) and density contrast (b), relative difference between prior and posterior model covariance matrix for magnetic susceptibility (c) and density contrast (d). The black dots show the edges of the two bodies modelled. The zones showing values close to zero on (b) and (d) correspond to the parts of the model where the model has been least updated by the joint inversion. Conversely, the anomalies are characterised by higher values in (b) and (d). The footprint of the main features of (b) and (d) is visible in (a) and (c). In contrast to what can be observed in (b) and (d) it seems that for magnetic susceptibility, higher resolution and variance reduction are limited to the shallow parts of the model. This could be due to sensitivity of the data to structures at depth decreasing more rapidly for magnetic data than for gravity data.

To analyse the agreement between the probability density function used in the petrophysical constraints and the results obtained from joint inversion we compute the cross-plot of the density contrast and magnetic susceptibility overlaid with chosen contour lines of the Gaussian MM of the rock model (see Figure 6).

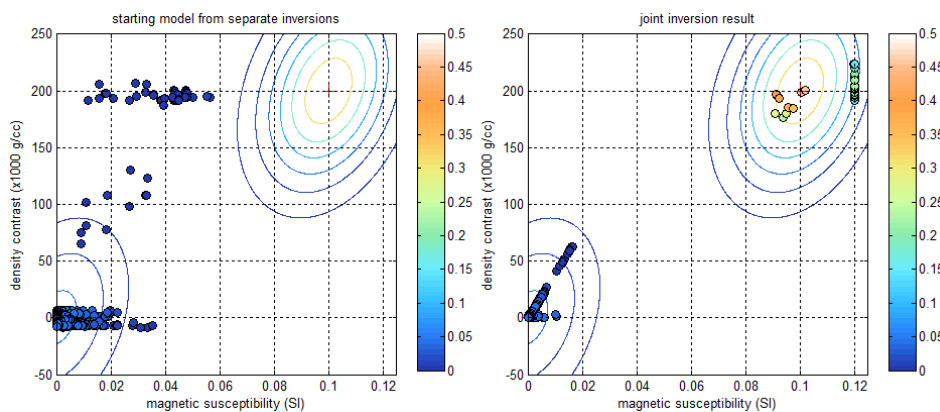


Figure 6: Cross-plot of magnetic susceptibility with density contrast overlaid with contour lines from the Gaussian Mixture Model used to apply to the petrophysical constraints. The results of the joint inversion show a much better agreement with the petrophysical constraints than the starting model, which was derived from single domain inversion.

From Figure 6 the probability of occurrence of the model obtained from joint inversion (right side of the Figure) is higher than from separate inversion (left side of the Figure). Figure 6 also shows that joint inversion enforced statistical consistency between the inverted model and the statistics of measured petrophysical data. In addition, Figure 5 shows an increase in the resolution of the model and a

decrease of the variances. Therefore, in this case, joint inversion is a good tool to reduce the uncertainty and increase the likelihood of the inverted model.

CONCLUSION AND DISCUSSION

In this abstract we have introduced a workflow that integrates several disciplines of the geosciences and shown its capacity to account for diverse sources of information to decrease the uncertainty on the result while being consistent with all the data. We have shown a synthetic example using the combination of petrophysical and geological data to constrain the joint inversion. However, only simple models have been tested. Further testing against more complex scenarios is planned. In addition, we have been simulating data for geophysical methods subject to similar physics: the potential field methods. Future work include the extension of the methodology introduced here to the joint inversion of gravity, magnetic and seismic data. Moreover, the benchmarking of this algorithm against other established workflows using a real case study is necessary to fully validate the methodology.

ACKNOWLEDGMENTS

The authors would like to acknowledge Desmond Fitzgerald for comments and constructive remarks at the beginning of this project. They would also like to acknowledge André Revil for interesting discussions about integration techniques and the use of prior information.

REFERENCES

- Colombo, D., and De Stefano, M., 2007, Geophysical modeling via simultaneous joint inversion of seismic, gravity and electromagnetic data: application to pre-stack depth imaging: *The Leading Edge*, March 2007, 326-331.
- Gallardo, L., and Meju, M. A., 2003, Characterization of heterogeneous near-surface materials by joint 2D inversion of dc resistivity and seismic data: *Geophysical Research Letters*, 30(13), 1-1 – 1-4.
- Gao, G., Abubakar, A., Habashy, T. M. and Pan, G., 2012, joint petrophysical inversion of electromagnetic and full-waveform seismic data: *Geophysics* 77(3), WA3-WA18.
- Garofalo, F., Sauvin, G., Socco, L. V. and Lecompte, I., 2015, Joint inversion of seismic and electric data applied to 2D media: *Geophysics*, 80 (4), EN93-EN104.
- Reid, A., O'Callaghan, S. T., Bonilla, E. V., McCalman, L., Rawling, T., and Ramos F., 2013, Bayesian Joint Inversions for the Exploration of Earth Resources: *Proceedings of the twenty-third international joint conference on artificial intelligence*, 2877-2884.
- Sun, J., and Li, Y., 2012, Joint inversion of multiple geophysical data: A petrophysical approach using guided fuzzy c-means clustering: *SEG Las Vegas 2012 Annual Meeting*, 1-5.
- Sun, J., and Li, Y., 2013, A general framework for joint inversion with petrophysical information as constraints: *SEG Houston 2013 Annual Meeting*, Houston, Expanded Abstracts, 3051-3056.
- Soueid Ahmed, A., Jardani A., Revil A., and Dupont, J. P., 2014, Hydraulic conductivity field characterization from the joint inversion of hydraulic heads and self-potential data: *Water Resources Research*, 50(4), 3502-3522.
- Tarantola, A., 1987, *Inverse problem theory: Methods for data fitting and model parameter estimation*: Elsevier Science.
- Tarantola, A., and Valette, B., 1982, Inverse Problems = Quest for Information: *Journal of Geophysics*, 50, 159-170.
- Zhang, J., and Revil, A., 2015, 2D joint inversion of geophysical data using petrophysical clustering and facies deformation: *Geophysics*, 80(5), M69-M88.